

Size Information Obtained Using Static Light Scattering Technique

Yong Sun

February 2, 2008

Abstract

Detailed investigation of static light scattering (*SLS*) has been attempted in this work using dilute water dispersions of homogenous spherical particles, poly(*N*-isopropylacrylamide) microgels and simulated data. When Rayleigh-Gans-Debye approximation is valid, for large particles, the simple size information, the static radius R_s and distribution $G(R_s)$, can be accurately obtained from SLS. For small particles, the root mean-square radius of gyration $\langle R_g^2 \rangle_{Zimm}^{1/2}$ and the molar mass of particles measured using the Zimm plot are discussed. The results show that the molar mass measured using the Zimm plot over the average molar mass of particles is a function of the size distribution. With the assistance of simulated data, the effects of the reflected light and noises have been investigated in detail. Measuring the static radius from the SLS data provides one method to avoid the stringent requirements for the sample quantity and the instrument capability at small scattering angles.

1 Introduction

The intensity of the scattered light is determined by the sizes, shapes and interaction among the particles in the scattering medium. During the last few decades, dynamic light scattering (*DLS*) is widely used to obtain the size information of particles for colloidal dispersion systems. Although the static light scattering (*SLS*) spectroscopy contains more sensitive size information, in general, the measurements of SLS spectroscopy are simplified to the Zimm plot, Berry plot or Guinier plot to obtain the root mean-square radius of gyration $\langle R_g^2 \rangle^{1/2}$ and the molar mass of particles provided that the particle sizes are small. Since it is hard to obtain the particle size distribution for small poly-disperse particles using DLS technique, for dilute poly-disperse homogeneous spherical particles, Pusey and van Megen [1] proposed a method to detect small poly-dispersities when the Rayleigh-Gans-Debye (*RGD*) approximation is valid, measuring the dependence of the effective diffusion coefficient obtained from the initial slope of the correlation function with respect to the scattering angle. By definition, the effective diffusion coefficient is the intensity-weighted average

diffusion coefficient. Both theoretical and experimental results show that the angular dependence of the effective diffusion coefficient is a sensitive function of the particle size and distribution.

How the particle size distributions can be obtained directly from the SLS data has been researched by a few authors. Hallett and Strawbridge [2] have studied the theoretical scattered intensity of a coated sphere with vertically polarized incident light. Then the scattered intensity at the geometrical or linear trial radii between r_{\min} and r_{\max} was used to fit the SLS data. Schnablegger and Glatter [3] assumed that the size distribution can be described as a series of cubic B-splines, then used the simulated and measured data to demonstrate the computation procedure.

In this article, we deal with the dilute poly-disperse homogeneous spherical particles. We assume that the number distribution of particles is Gaussian and we consider the effects of the form factor and the scattered intensity-weighted differences of different size particles on the scattered light intensity. Then with the assistance of a non-linear least squares fitting program, the mean particle size $\langle R_s \rangle$ and the standard deviation σ are obtained. With this treatment, we can avoid the constraints of the Zimm plot, Berry plot or Guinier plot on measurements, and their stringent dependences on sample quality and instrument capability at small angles. For large particles, size distributions can be measured accurately. With the assistance of simulated data, the effects of the reflected light and noises have been investigated in detail. Through the theoretical and simulated data analysis, the root mean-square radius of gyration $\langle R_g^2 \rangle_{Zimm}^{1/2}$ and the molar mass of particles measured using the Zimm plot are also discussed. The results show that the molar mass measured using the Zimm plot over the average molar mass of particles is a function of the size distribution. With theoretical and experimental data analysis, better understanding of the size information contained in SLS spectroscopies is obtained.

2 Theory

For simplicity, we consider homogeneous spherical particles and assume that the RGD approximation is valid. The average scattered light intensity of a dilute non-interacting polydisperse system in unit volume can be obtained for vertically polarized light

$$\frac{I_s}{I_{inc}} = \frac{4\pi^2 \sin^2 \theta_1 n_s^2 \left(\frac{dn}{dc}\right)_{c=0}^2 c 4\pi\rho \int_0^\infty R_s^6 P(q, R_s) G(R_s) dR_s}{\lambda^4 r^2 3 \int_0^\infty R_s^3 G(R_s) dR_s}, \quad (1)$$

where θ_1 is the angle between the polarization of the incident electric field and the propagation direction of the scattered field, c is the mass concentration of particles, r is the distance between the scattering particle and the point of the intensity measurement, ρ is the density of the particles, I_{inc} is the incident light intensity, I_s is the intensity of the scattered light that reaches the detector, R_s is a static radius of a particle, $q = \frac{4\pi}{\lambda} n_s \sin \frac{\theta}{2}$ is the scattering vector, λ is the

wavelength of the incident light in vacuo, n_s is the solvent refractive index, θ is the scattering angle, $P(q, R_s)$ is the form factor of homogeneous spherical particles

$$P(q, R_s) = \frac{9}{q^6 R_s^6} (\sin(qR_s) - qR_s \cos(qR_s))^2 \quad (2)$$

and $G(R_s)$ is the number distribution. In this paper, the number distribution is chosen as a Gaussian distribution

$$G(R_s; \langle R_s \rangle, \sigma) = \frac{1}{\sigma\sqrt{2\pi}} \exp\left(-\frac{1}{2} \left(\frac{R_s - \langle R_s \rangle}{\sigma}\right)^2\right), \quad (3)$$

where $\langle R_s \rangle$ is the mean static radius and σ is the standard deviation relative to the mean static radius.

If the reflected light is considered, the average scattered light intensity in unit volume is written as

$$\frac{I_s}{I_{inc}} = a \frac{4\pi\rho \int_0^\infty R_s^6 P(q, R_s) G(R_s) dR_s + b \int_0^\infty R_s^6 P(q', R_s) G(R_s) dR_s}{3 \int_0^\infty R_s^3 G(R_s) dR_s} \quad (4)$$

where

$$a = \frac{4\pi^2 \sin^2 \theta_1 n_s^2 \left(\frac{dn}{dc}\right)_{c=0}^2 c}{\lambda^4 r^2} \quad (5)$$

and

$$q' = \frac{4\pi}{\lambda} n_s \sin \frac{\pi - \theta}{2} \quad (6)$$

is the scattering vector of the reflected light. b is a constant decided by the shape of sample cell, the refractive indices of the solvent and the sample cell and the geometry of instruments.

When the values of qR_s are small, the form factor can be expanded and Eq. 1 can be written as

$$\frac{4\pi^2 \sin^2 \theta_1 n_s^2 \left(\frac{dn}{dc}\right)_{c=0}^2 c}{\lambda^4 r^2 N_0 \frac{I_s}{I_{inc}}} = \frac{\left(\int_0^\infty R_s^3 G(R_s) dR_s\right)^2}{\langle M \rangle \int_0^\infty R_s^6 G(R_s) dR_s} \left(1 + \frac{q^2 \int_0^\infty R_s^8 G(R_s) dR_s}{5 \int_0^\infty R_s^6 G(R_s) dR_s} + \dots\right) \quad (7)$$

where N_0 is the Avogadro's number, $\langle M \rangle$ is the average molar mass of particles. It is defined as

$$\langle M \rangle = \frac{4\pi\rho N_0}{3} \int_0^\infty R_s^3 G(R_s) dR_s. \quad (8)$$

Comparing with the Zimm plot analysis [[4] – [6]], the mean square radius of gyration, $\langle R_g^2 \rangle_{Zimm}$, for a polydisperse system is

$$\langle R_g^2 \rangle_{Zimm} = \frac{3 \int_0^\infty R_s^8 G(R_s) dR_s}{5 \int_0^\infty R_s^6 G(R_s) dR_s} \quad (9)$$

and the molar mass of particles measured using the Zimm plot is

$$M_z = \frac{\langle M \rangle \int_0^\infty R_s^6 G(R_s) dR_s}{\left(\int_0^\infty R_s^3 G(R_s) dR_s \right)^2}. \quad (10)$$

3 Experiment

The SLS spectroscopies were measured using the instrument built by ALV-Laser Vertriebsgesellschaft m.b.H (Langen, Germany). It utilizes an ALV-5000 Multiple Tau Digital Correlator and a JDS Uniphase 1145P He-Ne laser to provide a 23 mW vertically polarized laser at wavelength of 632.8 nm.

In this experiment, *N*-isopropylacrylamide (NIPAM, monomer) from Acros Organics was recrystallized from hexane/acetone solution. Potassium persulfate (KPS, initiator) and *N,N'*-methylenebisacrylamide (BIS, cross-linker) from Aldrich were used as received. Fresh de-ionized water from a Milli-Q Plus water purification system (Millipore, Bedford, with a 0.2 μm filter) was used throughout the whole experiment. The synthesis of gel particles was described elsewhere [[7], [8]] and the recipes of the batches used in this work are listed in Table 1.

Table 1. Synthesis conditions for PNIPAM particles.

Sample	T ($^{\circ}C$)	t (hrs)	$W_N + W_B$ (g)	KPS (mg)	n_B/n_N
<i>PNIPAM</i> – 0	70 ± 1	4.0	1.00	40	0
<i>PNIPAM</i> – 1	70 ± 1	4.0	1.00	40	1.0%
<i>PNIPAM</i> – 2	70 ± 1	4.0	1.00	40	2.0%
<i>PNIPAM</i> – 5	70 ± 1	4.0	1.00	40	5.0%

The four samples were named according to the molar ratios n_B/n_N of *N,N'*-methylenebisacrylamide over *N*-isopropylacrylamide. They were centrifuged at 14,500 RPM followed by decantation of the supernatants and re-dispersion in fresh de-ionized water four times to remove of free ions and any possible linear chains. Then the samples were diluted for light scattering to weight factors of 5.9×10^{-6} , 8.56×10^{-6} , 9.99×10^{-6} and 8.38×10^{-6} for *PNIPAM* – 0, *PNIPAM* – 1, *PNIPAM* – 2 and *PNIPAM* – 5 respectively. Before the measurements were made, 0.45 μm filters (Millipore, Bedford) were used to do dust free for the samples *PNIPAM* – 1, *PNIPAM* – 2 and *PNIPAM* – 5.

4 Data Analysis

How the size information is obtained from SLS is shown in this section. The experimental data of the *PNIPAM* microgel samples were used to show the fitting process and the simulated data were used to examine the effects of the different reflected light and the noises on the fit results and the effects of the distribution on the molar mass of particles measured using the Zimm plot.

4.1 Experimental Data Analysis

When Eq. 1 was fit to the data of *PNIPAM* – 1 measured at a temperature of $29^{\circ}C$, it was found that the results for mean static radii $\langle R_s \rangle$ and standard deviation σ depended on the scattering vector range being fit, as shown in Table 4.1. If a small scattering vector range is chosen, the parameters are not well-determined. As the scattering vector range is increased, χ^2 and the uncertainties in the parameters decrease and $\langle R_s \rangle$ and σ stabilize. If the fitting scattering vector range continues to increase, the values of $\langle R_s \rangle$ and σ begin to change and χ^2 grows. This is the result of the deviation between the experimental and theoretical scattered light intensity in the vicinity of the scattered intensity minimum. This minimum lies at about the scattering vector 0.0177 nm^{-1} . In this range, most of the scattered light is cancelled due to the light interference. So many other characteristics of particles can show the effects on the scattered light intensity, for example: the particle number distribution deviates from a Gaussian distribution, the particle shape deviates from a perfect sphere and the density of particles deviates from homogeneity, etc. In order to avoid the effects of light interference, the stable fit results during the scattering vector range from 0.00345 nm^{-1} to 0.01517 nm^{-1} are chosen as the size information obtained using the SLS technique. In order to examine the effects of the different fitting ranges of the scattering vector, the experimental data were fit again fixing the larger value of q and decreasing the fitting range. The fit results also are shown in Table 4.1. The values show the fit results are well-determined when the fitting range is enough large. Figure 4.1 shows the fit results and the residuals during the scattering vector range from 0.00345 nm^{-1} to 0.01517 nm^{-1} .

Table 4.1 The fit results for *PNIPAM*–1 in different scattering vector ranges and a temperature of $29^{\circ}C$.

$q (10^{-3} \text{ nm}^{-1})$	$\langle R_s \rangle (nm)$	$\sigma (nm)$	χ^2
3.45 to 9.05	260.09 ± 9.81	12.66 ± 19.81	1.64
3.45 to 11.18	260.30 ± 1.49	12.30 ± 3.37	1.65
3.45 to 13.23	253.45 ± 0.69	22.80 ± 0.94	2.26
3.45 to 14.21	254.10 ± 0.15	21.94 ± 0.36	2.03
3.45 to 15.17	254.34 ± 0.12	21.47 ± 0.33	2.15
3.45 to 17.00	255.40 ± 0.10	17.32 ± 0.22	11.02
5.50 to 15.17	254.24 ± 0.15	21.95 ± 0.47	2.32
7.95 to 15.17	254.32 ± 0.16	21.56 ± 0.57	2.38
10.12 to 15.17	254.65 ± 0.10	17.81 ± 0.63	0.79
12.21 to 15.17	254.84 ± 0.16	19.33 ± 0.87	0.42

If the reflected light was considered, Eq. 4 was used to fit all data in the full scattering vector range for various factors of reflected light b . The fit results are listed in Table 4.2. The fit results show that the values of χ^2 are too big, the value of mean static radius $\langle R_s \rangle$ is equal to that obtained using Eq. 1 in the fitting range with the small values of the scattering vector and the standard deviation changes to small.

Table 4.2 The fit results for *PNIPAM-1* were obtained using Eq. 4.

b	$\langle R_s \rangle (nm)$	$\sigma (nm)$	χ^2
0.01	254.0±0.3	14.4±0.5	194.60
0.011	254.0±0.3	14.6±0.5	168.20
0.012	254.0±0.3	14.7±0.5	149.99
0.013	254.0±0.2	14.8±0.4	139.82
0.014	254.1±0.2	15.0±0.4	137.52
0.015	254.1±0.2	15.1±0.4	142.96
0.016	254.09±0.07	15.2±0.5	155.97
0.017	254.1±0.3	15.4±0.5	176.40
0.018	254.1±0.3	15.5±0.5	204.08

As discussed above, light interference influences the fit results. In order to eliminate the effects of light interference, the experimental data in the vicinity of the scattered intensity minimum were neglected. Thus Eq. 4 was used to fit the experimental data in the full scattering vector range again. The fit values are shown in Table 4.3. The values can be thought to be consistent with the fit results obtained using Eq. 1 in the fitting range with the small values of the scattering vector .

Table 4.3 The fit results for *PNIPAM - 1* were obtained using Eq. 4 and neglecting some experimental data.

b	$\langle R_s \rangle (nm)$	$\sigma (nm)$	χ^2
0.013	251.3±0.6	22.17±0.05	79.80
0.014	251.1±0.6	23.3±0.9	58.29
0.015	250.9±0.6	24.4±0.8	44.50
0.016	250.7±0.5	25.4±0.7	37.02
0.017	250.5±0.6	26.4±0.7	36.01
0.018	250.3±0.6	27.24±0.8	41.59

Because 0.45 μm filters were used to do dust free for our samples, we can think that the very big particles do not exist. So the expected values calculated using Eq. 4 and the fit results obtained using Eq. 1 over the fitting range from 0.00345 nm^{-1} to 0.01517 nm^{-1} can be consistent with the experimental data if the number distribution was corrected. The expected values calculated in three different situations for *PNIPAM - 1* are shown in Fig. 4.2. First, the expected results of the incident light calculated during the full particle size distribution range. Next, a truncated Gaussian was used, ie. integrated between about the $\langle R_s \rangle - 1.3\sigma$ and $\langle R_s \rangle + 1.3\sigma$ instead of between 1 and 800 nm and the expected values of the incident light were thus calculated in this truncated Gaussian distribution. Finally, the integrated range is the same as the second, the expected values of the incident and the reflected light were calculated with b : 0.014. That the expected values in the third are consistent with the experimental data show the average scattered intensity is very sensitive to the particle size distribution.

For the particles with small sizes, the fit results are shown in Table 4.4. The sample is *PNIPAM - 5*. The data were measured at a temperature of 40°C.

The fit results during the scattering vector range from 0.00345 nm^{-1} to 0.02555 nm^{-1} are chosen as the size information obtained using the SLS technique since the values of $\langle R_s \rangle$ and σ stabilize. Figure 4.3 shows the fit results and the residuals during the scattering vector range from 0.00345 nm^{-1} to 0.02555 nm^{-1} .

Table 4.4 The fit results for *PNIPAM-5* at different scattering vector ranges and a temperature of 40°C .

$q \text{ (} 10^{-3} \text{ nm}^{-1} \text{)}$	$\langle R_s \rangle \text{ (nm)}$	$\sigma \text{ (nm)}$	χ^2
3.45 to 14.21	143.78 ± 8.34	7.32 ± 14.78	2.68
3.45 to 16.10	116.70 ± 7.35	27.01 ± 3.40	2.97
3.45 to 17.87	130.01 ± 3.54	19.45 ± 2.41	2.92
3.45 to 19.50	142.29 ± 2.33	7.26 ± 4.48	4.43
3.45 to 20.98	138.18 ± 1.50	13.47 ± 1.57	3.97
3.45 to 23.46	142.30 ± 0.57	7.97 ± 1.22	3.18
3.45 to 24.44	140.09 ± 0.46	11.59 ± 0.73	3.66
3.45 to 25.23	139.57 ± 0.41	12.33 ± 0.63	3.87
3.45 to 25.55	139.34 ± 0.31	12.36 ± 0.55	5.50

For *PNIPAM-5*, due to the values of qR_s are small, so the Zimm plot can be used to obtain the approximative value of the root mean square radius of gyration $\langle R_g^2 \rangle_{Zimm}^{1/2}$. The results of the Zimm plot is shown in Fig. 4.4. The value of $\langle R_g^2 \rangle_{Zimm}^{1/2}$ is about 115.55 nm .

4.2 Simulated Data Analysis

In order to conveniently discuss the effects of the reflected light and the noises, the simulated data have been produced with a Gaussian distribution.

4.2.1 Simulated data of large particles

For large particles, both the effects of the reflected light and the noises must be considered. First, the effects of the reflected light are considered. The simulated data of the incident light were produced using Eq. 1 and the data of the reflected light were obtained using the following equation

$$\frac{I_s}{I_{inc}} = a \frac{4\pi\rho b \int_0^\infty R_s^6 P(q', R_s) G(R_s) dR_s}{3 \int_0^\infty R_s^3 G(R_s) dR_s}. \quad (11)$$

Then the 1% statistical noises were added to the simulated data respectively. Next we will keep the simulated data and only consider the effects of the reflected light.

The scattered intensity of the reflected light was added to the total scattered intensities. When the final data of $\frac{I_s}{I_{inc}}$ were obtained, the 3% random errors were set. The simulated data 1 was produced when the mean radius was set 267 nm and the standard deviation was 23 nm . The fit results using Eq. 1 at different scattering vector ranges are listed in Table 4.5 for the value of b was

chosen to be 0.015. The results show that the fit results' errors decrease and the mean radius and the standard deviation stabilize when the fitting scattering vector range is enlarged. Figure 4.5 shows the fit results and the residuals during the scattering vector range from 0.00345 nm^{-1} to 0.01592 nm^{-1} .

Table 4.5 The fit results for the simulated data 1 with $b: 0.015$ at different scattering vector ranges.

$q \text{ (} 10^{-3} \text{ nm}^{-1} \text{)}$	$\langle R_s \rangle \text{ (nm)}$	$\sigma \text{ (nm)}$	χ^2
3.45 to 10.97	272.52 ± 1.76	12.97 ± 4.56	0.81
3.45 to 12.01	271.18 ± 1.06	16.00 ± 2.30	0.75
3.45 to 13.02	269.41 ± 0.68	19.40 ± 1.25	0.76
3.45 to 14.02	267.45 ± 0.22	22.64 ± 0.42	0.82
3.45 to 14.98	266.95 ± 0.03	23.53 ± 0.17	0.88
3.45 to 15.92	266.96 ± 0.02	23.45 ± 0.09	0.82

Since the Gaussian distribution was used to produce the simulated data, so Eq. 4 can be used to fit the data at the full scattering vector range. The fit results with the various values of b are listed in Table 4.6. The fit results are consistent with those obtained using Eq. 1 in the fitting range with the small values of the scattering vector.

Table 4.6 The fit results for the simulated data 1 with $b: 0.015$ were obtained using Eq. 4.

b	$\langle R_s \rangle \text{ (nm)}$	$\sigma \text{ (nm)}$	χ^2
0.012	266.62 ± 0.22	22.80 ± 0.24	28.06
0.013	266.67 ± 0.15	22.91 ± 0.17	13.64
0.014	266.72 ± 0.09	23.01 ± 0.098	4.73
0.015	266.758 ± 0.001	23.14 ± 0.03	1.00
0.016	266.83 ± 0.07	23.22 ± 0.08	2.76
0.017	266.89 ± 0.13	23.32 ± 0.14	9.39
0.018	266.95 ± 0.198	23.43 ± 0.21	20.87

The fit results obtained using Eq. 1 in the scattering vector range from 0.00345 nm^{-1} to 0.01592 nm^{-1} were input Eq. 1 and Eq. 4 to calculate the expected values at the full scattering vector range with $b: 0.015$, respectively. The results are shown in Fig. 4.6. The expected results are consistent with the simulated data.

In order to investigate the effects of the reflected light on the fit results obtained using Eq. 1 in a fitting range with the small values of the scattering vector. The simulated data were produced for $b=0.0, 0.005, 0.01$ and 0.02 respectively. The fit results at the same scattering vector range from 0.00345 nm^{-1} to 0.01592 nm^{-1} are listed in Table 4.7. The fit values show that the size information can be accurately obtained using Eq. 1 in the fitting range with the small values of the scattering vector and the effects of the reflected light do not need to be considered.

Table 4.7 The fit results for the simulative data 1 with the different reflected light.

b	$\langle R_s \rangle (nm)$	$\sigma(nm)$	χ^2
0	267.15±0.02	23.103±0.09	0.84
0.005	267.08±0.02	23.22±0.09	0.82
0.01	267.01±0.02	23.42±0.13	0.83
0.015	266.96±0.02	23.45±0.09	0.82
0.020	266.89±0.02	23.56±0.09	0.83

Second, the effects of noises will be considered. The fit results of simulated data 1 with different noises and the various values of b in the scattering vector range from 0.00345 nm^{-1} to 0.01592 nm^{-1} are shown in Table 4.8. The results show that the noises do not influence the fit values.

Table 4.8 The fit results for the simulated data 1 with the different noises and reflected light.

	$\langle R_s \rangle (nm)$	$\sigma(nm)$	χ^2
0	267.141±0.001	23.09±0.06	1.20
0.005	266.91±0.07	23.2±0.1	1.55
0.01	266.82±0.03	23.30±0.04	0.61
0.015	266.95±0.03	23.736±0.08	1.71
0.02	266.82±0.04	23.6±0.2	2.91

4.2.2 Simulated data of small particles

For small particles, only the effects of noises need to be considered. The simulated data 2 was produced when the mean radius was set 90 nm and the standard deviation was 7 nm . The final simulated data were obtained in two different situations: one is that the noises were not added (*first*) and the other is that the 1% statistical noises were added (second to fifth). The fit results are listed in Table 4.9. The values show that the fit results are influenced by noises. Figure 4.7 shows the fit results and residuals for the fifth simulated data of the simulated data 2.

Table 4.9 The fit results for the simulated data 2 with different noises.

	$\langle R_s \rangle (nm)$	$\sigma(nm)$	χ^2
First	89.97±0.08	7.02±0.09	0.004
Second	87.2±3.0	10.5±2.5	1.41
Third	79.0±3.4	15.4±1.7	2.02
Fourth	77.5±2.3	16.2±1.2	0.84
Fifth	91.2±1.2	4.9±2.0	1.94

If the simulated data 2 with the different noises are put together, as shown in Fig. 4.8, the differences among the simulated data 2 with the different noises cannot be distinguished. From the Zimm plot analysis, the root mean square radius of gyration $\langle R_g^2 \rangle_{Zimm}^{1/2}$ and the Zimm's molar mass of the particles will be the same. However, due to the size distribution, the average molar mass of particles $\langle M \rangle$ will have large differences for the particles with different distributions. Figure 4.9 shows the results using the Zimm plot to fit the third simulated data of the simulated data 2. For the five simulated data, the fit

values of $\langle R_g^2 \rangle_{Zimm}^{1/2}$ are listed in Table 4.10. If the symbol k is used to represent the quantity $M_z/\langle M \rangle$. The expected values of $\langle R_g^2 \rangle_{cal}^{1/2}$ and k obtained using Eqs. 9 and 10 are also shown in Table 4.10.

Table 4.10 Values of $\langle R_g^2 \rangle_{Zimm}^{1/2}$, $\langle R_g^2 \rangle_{cal}^{1/2}$ and k .

	$\langle R_g^2 \rangle_{Zimm}^{1/2} (nm)$	$\langle R_g^2 \rangle_{cal}^{1/2} (nm)$	k
First	74.96	72.36	1.05
Second	75.46	73.46	1.13
Third	73.67	73.97	1.32
Fourth	73.12	74.17	1.36
Fifth	74.96	71.95	1.03

Since the value of k has a strong dependence on the distribution of particles, the simulated data 3 was produced as the simulated data 2 with a mean static radius 50 nm and a standard deviation 10 nm. The fit results are listed in Table 4.11. The fit values of $\langle R_g^2 \rangle_{Zimm}^{1/2}$, the expected values of $\langle R_g^2 \rangle_{cal}^{1/2}$ and k are shown in Table 4.12.

Table 4.11 The fit results for the simulated data 3 with different noises.

	$\langle R_s \rangle (nm)$	$\sigma(nm)$	χ^2
First	50.5±0.2	9.76±0.08	9.9*10 ⁻⁵
Second	57.3±3.2	5.1±3.0	0.46
Third	42.3±5.4	12.5±1.9	3.39
Fourth	58.7±0.8	3.9±0.9	0.30
Fifth	58.96±0.01	3.6±0.2	2.57

Table 4.12 Values of $\langle R_g^2 \rangle_{Zimm}^{1/2}$, $\langle R_g^2 \rangle_{cal}^{1/2}$ and k .

	$\langle R_g^2 \rangle_{Zimm}^{1/2} (nm)$	$\langle R_g^2 \rangle_{cal}^{1/2} (nm)$	k
First	48.41	47.17	1.31
Second	48.40	46.58	1.07
Third	47.72	46.36	1.67
Fourth	48.47	46.74	1.04
Fifth	46.34	46.75	1.03

5 Results and Discussion

From the analysis of simulated data, for large particles, the reflected light and the noises do not need to be considered when the size information is obtained from the SLS data in the fitting range with the small values of the scattering vector. We ever produced the simulated data for the wide distributions and much larger sizes. The conclusion is the same. For wide distributions, the mean radius 267 nm and the standard deviation 134 nm were used to produce the simulated data, the fit results during the scattering vector range 0.00345 nm⁻¹ to 0.01498 nm⁻¹ are that the mean radius is 267.5±0.9 nm, the standard deviation is 134.2±0.5 nm and χ^2 is 0.91. The expected values calculated inputting the results in Eqs. 1 and 4 respectively are shown in Fig. 5.1.

For the much larger size, the mean radius 500 nm and the standard deviation 15 nm were used to produce the simulated data, the fit results during the scattering vector range from 0.00345 nm⁻¹ to 0.00969 nm⁻¹ are that the mean radius is 500.10±0.04 nm, the standard deviation is 15.20±0.04 nm and χ^2 is 0.37. The expected values calculated inputting the results in Eqs. 1 and 4 respectively are shown in Fig. 5.2.

How the values of $\langle R_g^2 \rangle_{Zimm}^{1/2}$ can be obtained has been shown. The fit results choosing the different data points for the simulated data 2 are listed in Table 5.1. The results show that the values almost keep a constant for the different fitting ranges.

Table 5.1 The values of $\langle R_g^2 \rangle_{Zimm}^{1/2}$ of the simulated data 2 with the different noises.

$\langle R_g^2 \rangle_{Zimm}^{1/2} (nm)$					
Fit points	First	Second	Third	Fourth	Fifth
1 to 15	74.46	70.60	73.16	74.62	78.19
1 to 20	74.96	75.50	73.67	73.13	74.96
1 to 25	75.62	76.26	75.99	75.12	74.65
1 to 30	76.43	77.58	77.46	77.73	75.64
1 to 35	77.28	77.76	77.61	78.07	76.48

Since the sizes of PNIPAM microgel particles at high temperatures are small, the fit values will be influenced by noises, but this method still can give the better values of $\langle R_g^2 \rangle_{Zimm}^{1/2}$ and make us avoid the stringent requirements for the sample quality and the instrument capability at smaller scattering angles. The fit values of the four PNIPAM microgel samples at high temperatures are listed in Table 5.2. All the experimental data of *PNIPAM* – 5 and the results obtained using the Zimm plot in a range with the small values of the scattering vector are shown in Fig. 5.3. The picture shows that the values of $\langle R_g^2 \rangle_{Zimm}^{1/2}$ obtained using a Zimm plot have a large uncertainty. The value is determined by the chosen data. Even if the data points that obviously deviate from the linear range were neglected, the values of $\langle R_g^2 \rangle_{Zimm}^{1/2}$ still show a strong dependence on the fit points. For the four PNIPAM microgel samples, the fit results obtained from a Zimm plot analysis are shown in Table 5.3.

Table 5.2 The fit results for the four PNIPAM microgel samples at high temperatures.

Sample (<i>Temperature</i>)	$\langle R_s \rangle (nm)$	$\sigma (nm)$	χ^2
<i>PNIPAM</i> – 5 (40°C)	139.3±0.3	12.4±0.6	5.50
<i>PNIPAM</i> – 2 (40°C)	114.4±0.9	11.4±1.1	4.34
<i>PNIPAM</i> – 1 (40°C)	111.7±0.9	14.8±0.8	2.73
<i>PNIPAM</i> – 0 (40°C)	101.7±1.1	8.6±1.3	1.80
<i>PNIPAM</i> – 0 (34°C)	93.4±1.9	24.5±0.9	1.56

The fit values for the experimental data of the four PNIPAM microgel samples measured at high temperatures were input to Eqs. 9 and 10 respectively to obtain the expected values of $\langle R_g^2 \rangle_{cal}^{1/2}$ and k . The values are listed in Table 5.3.

Table 5.3 Values of $\langle R_g^2 \rangle_{cal}^{1/2}$, $\langle R_g^2 \rangle_{Zimm}^{1/2}$ and k for the four PNIPAM microgel samples at high temperatures.

Sample (<i>Temperature</i>)	$\langle R_g^2 \rangle_{cal}^{1/2}$ (nm)	$\langle R_g^2 \rangle_{Zimm}^{1/2}$ (nm)	k
PNIPAM – 5 (40°C)	113.23	113.73 to 122.85	1.07
PNIPAM – 2 (40°C)	94.05	89.39 to 125.89	1.09
PNIPAM – 1 (40°C)	95.58	88.62 to 164.87	1.15
PNIPAM – 0 (40°C)	82.28	74.78 to 86.36	1.06
PNIPAM – 0 (34°C)	97.15	102.48 to 113.06	1.55

6 Conclusion

The consistency between the theoretical results and SLS data shows that the size information can be obtained using the non-linear least squares fitting method and the SLS data contain sensitive size information of particles. For the large particles, the reflected light and the noises do not influence the fit results in the range with the small values of the scattering vector. Eq. 1 provides a method to measure accurately the particle size distribution and makes it possible to measure the average molar mass of large particles if the absolute magnitude of the scattered intensity and some constants that are related to the instrument and samples are known.

For small size particles, although the fit values are influenced by noises, it still is a good method to obtain the size information from the SLS data. It can give a better approximative value of $\langle R_g^2 \rangle_{Zimm}^{1/2}$ and avoid the stringent dependences on the sample quantity and the instrument capability. The molar mass of particles obtained using the Zimm plot is a better approximative value of the average molar mass of particles only for the particle systems with very narrow distributions.

The simple number distributions $G(R_s)$ obtained from the SLS data are the distributions that people really want to obtain from the experimental data. They make us avoid the other parameters' effects when the effects of particle sizes are analyzed.

Fig. 4.1 The experimental and fit results for *PNIPAM* – 1 at a temperature of 29°C. The circles show the experimental data, the line shows the fit results and the diamonds show the residuals: $(y_i - y_{fit})/\sigma_i$.

Fig. 4.2 The experimental and expected results for *PNIPAM* – 1. The circles show the experimental data, the line shows the expected results of the incident light calculated during the full particle size distribution range, the dash dot line represents the expected results of the incident light calculated between about the $\langle R_s \rangle - 1.3\sigma$ and $\langle R_s \rangle + 1.3\sigma$ and the dot line shows the expected results of the incident and the reflected light calculated in the same range as the second with b : 0.014.

Fig. 4.3 The experimental and fit results for *PNIPAM* – 5 at a temperature of 40°C. The circles show the experimental data, the line shows the fit results and the diamonds show the residuals: $(y_i - y_{fit})/\sigma_i$.

Fig. 4.4 The results of a Zimm plot for *PNIPAM* – 5 at a temperature of 40°C . The circles show the experimental data and the line shows a linear fit to the plot of Kc/R_{vv} as a function of q^2 .

Fig. 4.5 The simulated and fit results for the simulated data 1 with b : 0.015. The circles show the simulated data, the line shows the fit results and the diamonds show the residuals: $(y_i - y_{fit})/\sigma_i$.

Fig. 4.6 The simulated and expected results for the simulated data 1 with b : 0.015. The circles show the simulated data, the line shows the expected results of the incident light calculated during the full particle size distribution range and the dot line shows the expected results of the incident and reflected light calculated during the full particle size distribution range with b : 0.015.

Fig. 4.7 The simulated and fit results for the fifth simulated data of the simulated data 2. The circles show the simulated data, the line shows the fit results and the diamonds show the residuals: $(y_i - y_{fit})/\sigma_i$.

Fig. 4.8 The simulated data 2 with the different noises.

Fig. 4.9 The results of a Zimm plot for the third simulated data of the simulated data 2. The circles show the simulated data and the line shows a linear fit to the plot of I_{inc}/I_s as a function of q^2 .

Fig. 5.1 The simulated and expected results for the simulated data. The circles show the simulated data, the line shows the expected results of the incident light calculated during the full particle size distribution range and the dot line shows the expected results of the incident and reflected light calculated during the full particle size distribution range with b : 0.01.

Fig. 5.2 The simulated and expected results for the simulated data. The circles show the simulated data, the line shows the expected results of the incident light calculated during the full particle size distribution range and the dot line shows the expected results of the incident and reflected light calculated during the full particle size distribution range with b : 0.01.

Fig. 5.3 The results of the Zimm plot and the experimental data for *PNIPAM* – 5 at a temperature of 40°C in a large scattering vector range. The circles show the experimental data and the line shows the results of a Zimm plot obtained in a range with the small values of the scattering vector.

References

- [1] P. N. Pusey and W. van Megen, *J. Chem. Phys.*, 1984, 80, 3513
- [2] K. B. Strawbridge and F. R. Hallett, *Macromolecules*, 1994, 27, 2283
- [3] H. Schnablegger and O. Glatter, *J. Colloid. Interface Sci.* 1993, 158, 228
- [4] B. H. Zimm, *J. Chem. Phys.* 1948, 16, 1099
- [5] W. Burchard, *Adv. Polym. Sci.* 1983, 48, 1
- [6] B. Chu, *Laser Light Scattering: Basic Principles and Practice*, Academic Press, Inc. New York, 1991

[7] J. Gao and B. J. Frisken, *Langmuir*, 2003, 19, 5217

[8] J. Gao and B. J. Frisken, *Langmuir*, 2003, 19, 5212

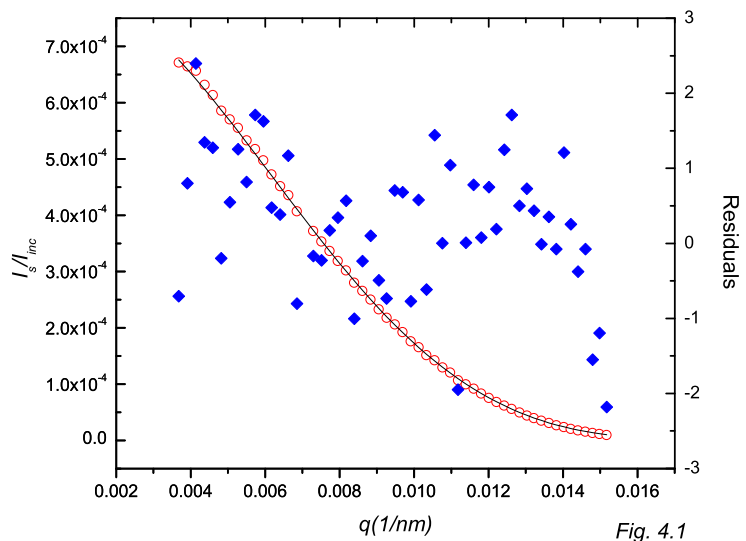


Fig. 4.1

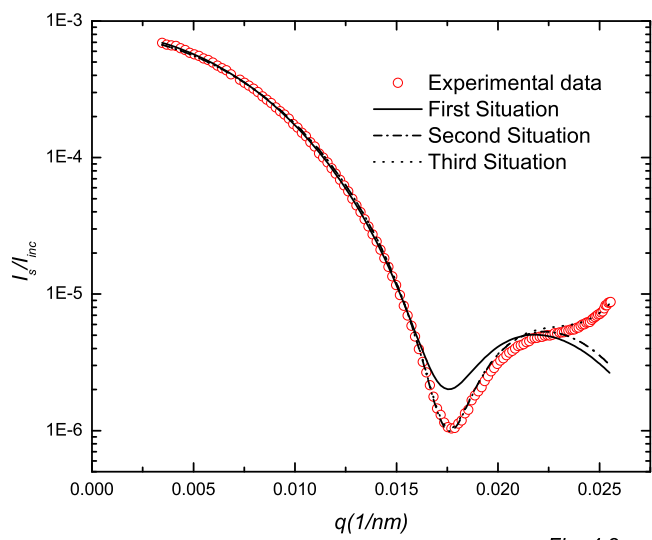


Fig. 4.2

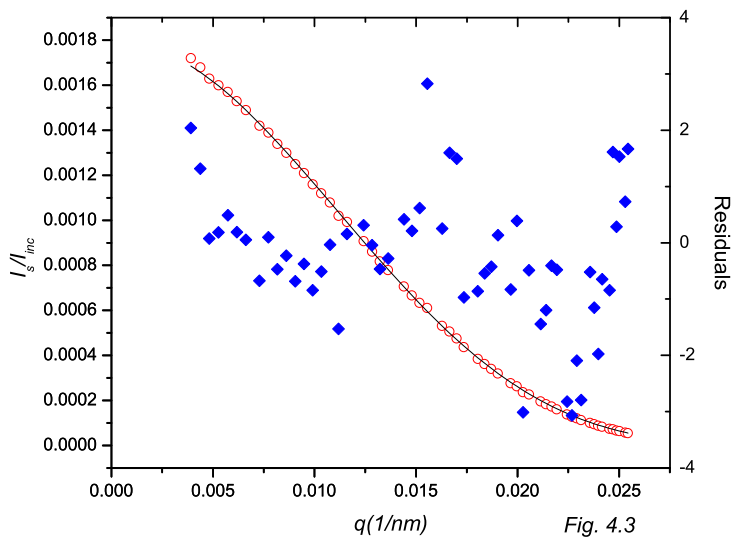


Fig. 4.3

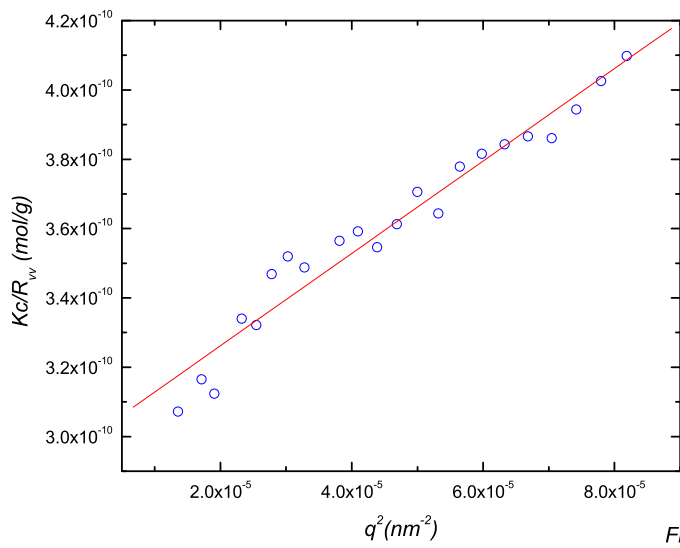


Fig. 4.4

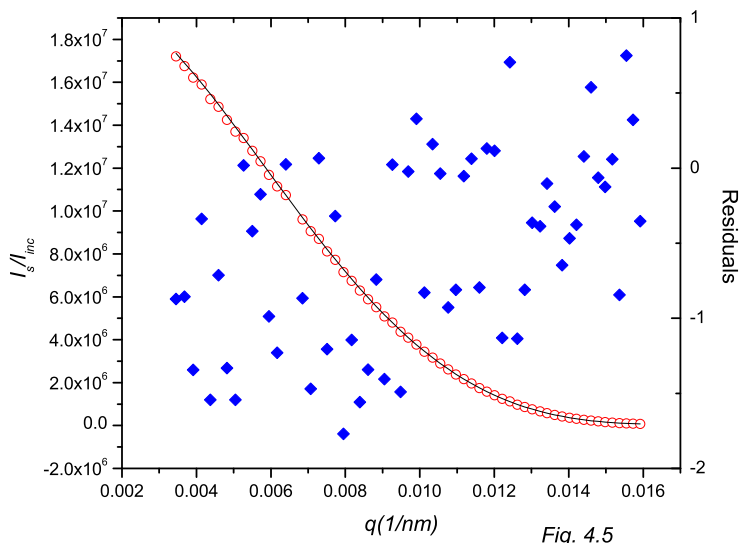


Fig. 4.5

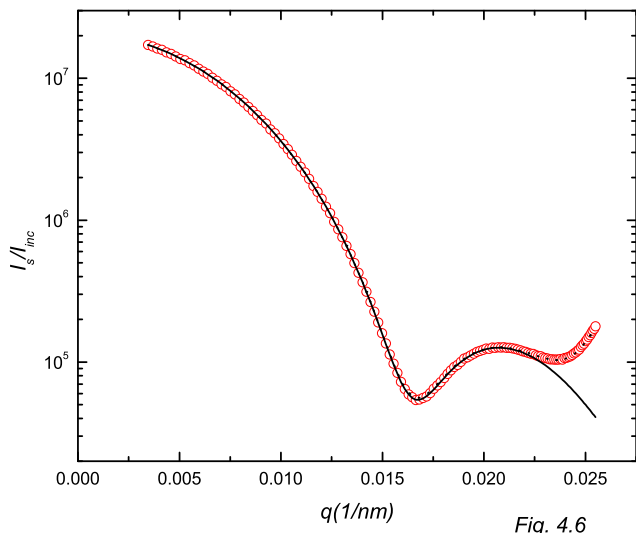


Fig. 4.6

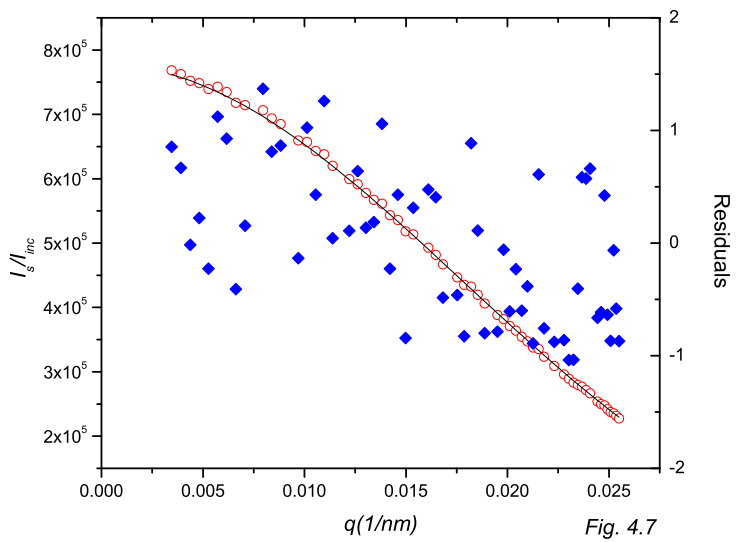


Fig. 4.7

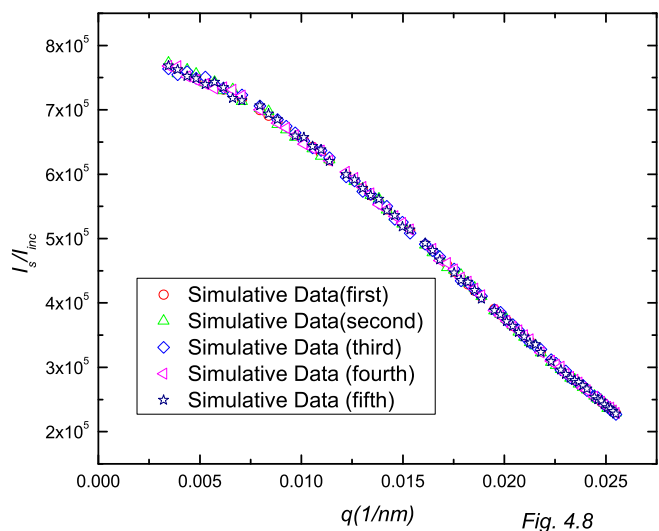


Fig. 4.8

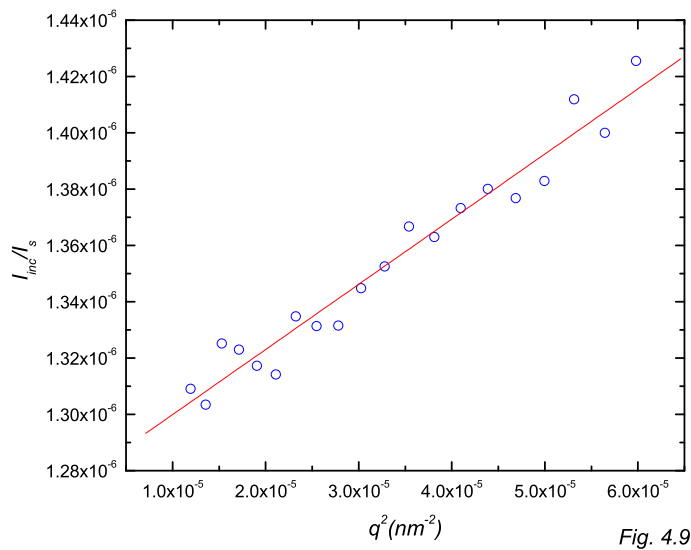


Fig. 4.9

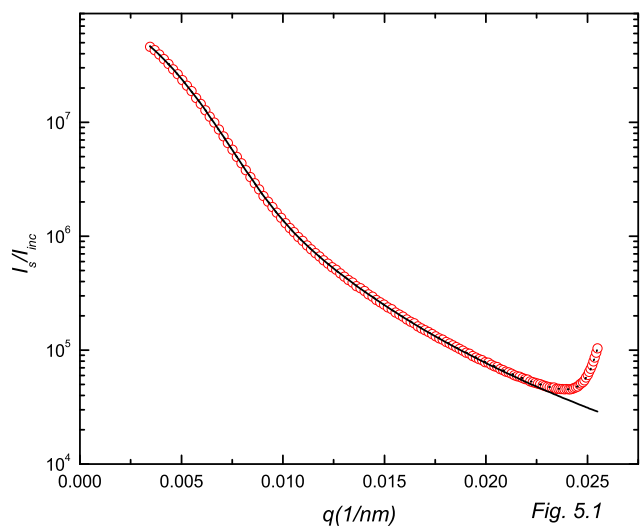


Fig. 5.1

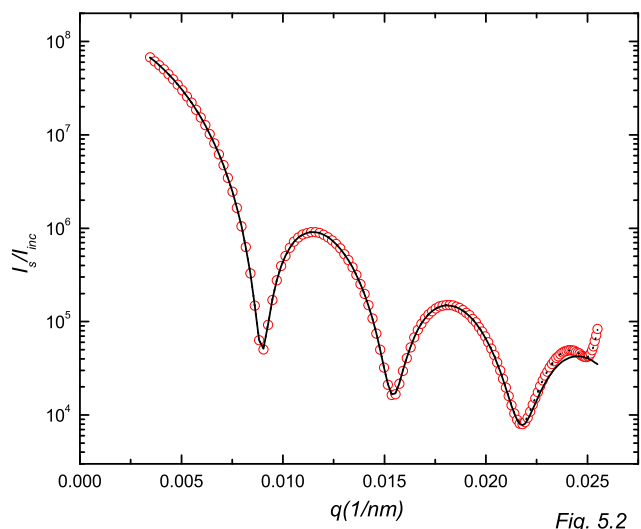


Fig. 5.2

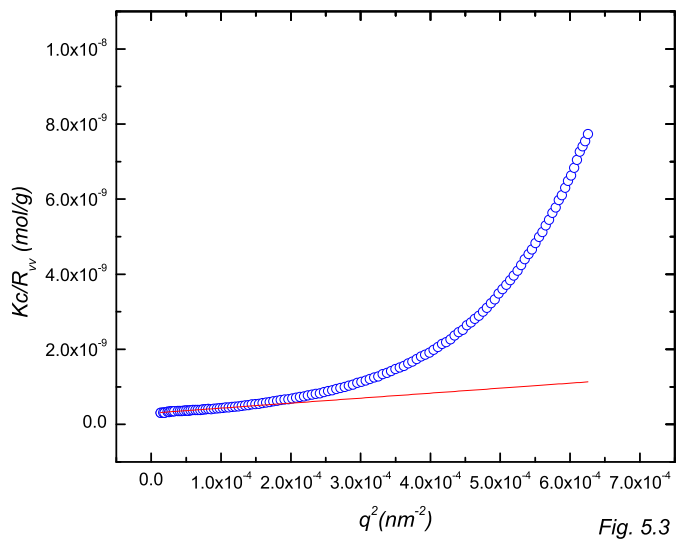


Fig. 5.3